

LA-UR-79-646

TITLE: CALCULATION OF EXPLOSIVE ROCK BREAKAGE: OIL SHALE

AUTHOR(S): J. N. Johnson

SUBMITTED TO: 20th U.S. Symposium on Rock Mechanics
University of Texas at Austin
June 3-6 1979

NOTICE
This report was prepared as an account of work sponsored by the United States Government. Neither the United States nor the United States Department of Energy, nor any of their employees, nor any of their contractors, subcontractors, or their employees, makes any warranty, express or implied, or assumes any legal liability or responsibility for the accuracy, completeness or usefulness of any information, apparatus, product or process disclosed, or represents that its use would not infringe privately owned rights.

By acceptance of this article for publication, the publisher recognizes the Government's (license) rights in any copyright and the Government and its authorized representatives have unrestricted right to reproduce in whole or in part said article under any copyright secured by the publisher.

The Los Alamos Scientific Laboratory requests that the publisher identify this article as work performed under the auspices of the USERDA.


los alamos
scientific laboratory
of the University of California
LOS ALAMOS, NEW MEXICO 87545

An Affirmative Action/Equal Opportunity Employer

MASTER

CALCULATION OF EXPLOSIVE ROCK BREAKAGE: OIL SHALE

J. N. Johnson, Los Alamos Scientific Laboratory

ABSTRACT

Improved efficiency in explosive rock breakage becomes increasingly important as mining costs and the need to tap underground resources continue to grow. Industry has recognized this need for many years and has done a great deal in developing new products and new blasting techniques, generally by purely empirical means. One particular application that has received added attention within the past several years, and one that lends itself to a more objective theoretical study, is explosive fracture of oil shale for conventional and *in situ* fossil energy recovery.

Numerical calculation of oil shale fracturization with commercial explosives has the potential to add to an objective understanding of the breakage process. Often, in such numerical studies, only one or two parts of the total problem are addressed with any degree of sophistication or completeness. Here an attempt is made to treat the entire problem, i.e., explosive characterization, constitutive behavior of intact rock, and a mathematical description of rock fracture. The final results are two-dimensional calculations of explosively induced fracture damage in oil shale.

INTRODUCTION

A subject of current national interest is energy and mineral resource recovery, and an important part of this subject is controlled rock blasting with commercial explosives. Explosive rock blasting has been studied empirically by a number of investigators.¹⁻⁵ Generally, these studies consist of developing empirical relationships between rock blasting efficiency and detonation velocity, energy release, expansion work, etc. The reason for such an approach is that detailed consideration of actual explosive performance, coupled with high-, intermediate-, and low-strain-rate fracture mechanics to predict actual removal of rock from a blasting face, is an extremely difficult problem. However, as our predictive capabilities in dynamic rock fracture continue to improve, it becomes

possible to perform useful numerical calculations of explosively induced rock breakage, provided that a data base and the corresponding mathematical models are established for the following three aspects of the problem: (1) performance properties of commercial explosives, (2) constitutive properties of intact rock, and (3) the failure surface and post-failure constitutive properties of fractured rock.

In this paper an attempt is made to address all three aspects of the problem. Experimental and theoretical results are given on the performance properties of one of the most widely used commercial explosives, ANFO (Ammonium Nitrate/Fuel Oil mixture), in cylindrical geometry at 10 cm, 20 cm, and ≤ 30 cm diameter. This is followed by a summary of the mechanical properties of intact oil shale as functions of initial density or, equivalently, kerogen content. The stress states for which failure occurs and the post-failure properties of fractured rock are defined in terms of a yield surface and a single scalar parameter D , termed the "damage," which goes from 0 for intact rock to 1 for fully fractured rock. Finally, two-dimensional finite-difference calculations based on these data and models are performed for explosive fracture of oil shale in cylindrical (cratering) and planar (bench blasting) geometries.

The underlying goal of this work is to develop improved descriptions of explosive rock breakage based on first principles, or as near to first principles as is currently practical.

NONIDEAL EXPLOSIVE CHARACTERIZATION

Many explosives systems have been studied extensively and their behavior is extremely well understood. However, when explosive performance closely follows theoretical behavior (we say the explosive behaves ideally), economic considerations often limit applicability because of the cost of the great quantities of explosive needed on a commercial scale. On the other hand, commercially available explosives are inexpensive but usually do not behave according to steady-state theoretical

References and illustrations at end of paper.

predictions based on equilibrium thermodynamics of the expected detonation products (such explosives exhibit nonideal behavior). Therefore, for non-ideal commercial explosive systems, extensive measurement of several performance parameters are necessary to assess correctly the actual behavior and departure from ideal conditions. Because the performance of commercial explosives is geometry and confinement dependent, it is important to test them under conditions that closely approximate actual field applications.

Experimental and theoretical results are presented here for the characterization of ANFO (Ammonium Nitrate/Fuel Oil, approximately 94 wt%/6 wt%) at a nominal density of 0.9 g/cm^3 in cylindrical geometry with Plexiglas and clay confinement. This work (explosive characterization) is described in detail in Ref. 6.

Preliminary rate-stick experiments (confined cylindrical specimens in which detonation velocity along the cylinder axis is measured) show that ANFO does not undergo high-order detonation for diameters less than $\sim 7.5 \text{ cm}$ with Plexiglas confinement.⁶ The measured detonation velocity for a 10-cm-diameter specimen with Plexiglas confinement was 3.5 km/s . The 10-cm-diameter test detonated high order as determined by ionization pin measurements.

Rate-stick experiments give detonation velocity as well as information on the effects of confinement and charge diameter, but they do not provide a quantitative understanding of the physical and chemical phenomena occurring behind the detonation front. Therefore, the water-tank experiment was developed to measure simultaneously detonation velocity and pressure, confinement effects, and the release isentrope from the Chapman-Jouguet (C-J) state. Figure 1 shows a schematic diagram of the experimental setup for the HE/water-tank experiments. A confined cylinder of explosive is detonated from one end in water.

The data consist of measured radial positions of the confinement tube and the water shock as functions of position behind the detonation front photographed with an image-intensifier camera (I²C).⁷ Two-dimensional hydrodynamic calculations of the aquarium shots are then performed and compared with experimental data, giving considerable information on the actual explosive performance. This method is similar to that used in performance studies of other nonideal explosive systems.⁸⁻¹³

The experimental I²C record for shot C-4632, a 100-cm-diameter cylinder of ANFO with Plexiglas confinement, is shown in Fig. 2.

For shots C-4632 (10-cm-diameter ANFO with Plexiglas confinement) and C-4652 (10-cm-diameter ANFO with clay-pipe confinement), the detonation velocities are almost identical: 3.48 km/s and 3.47 km/s , respectively. This indicates that details of the type of confinement are not important in this configuration, as long as the sound speed in the confining medium is less than the detonation velocity. In fact, it is concluded that the confinement provided by both the Plexiglas/water and clay/water systems is equivalent to an infinite medium with mechanical properties representative of typical rocks. It is also noted that the measured detonation velocity is somewhat less than the value

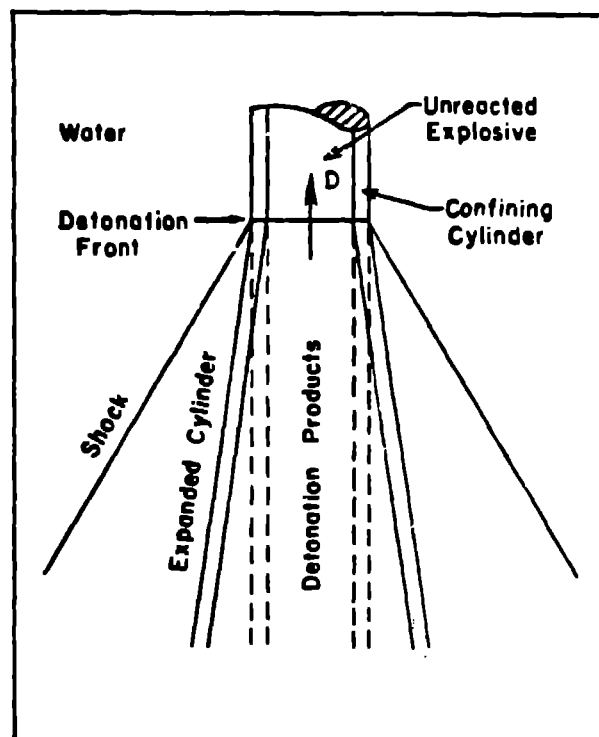


Fig. 1. Positions of bubble and shock fronts resulting from a detonation wave of velocity D propagating down an explosive cylinder immersed in a transparent confining fluid.

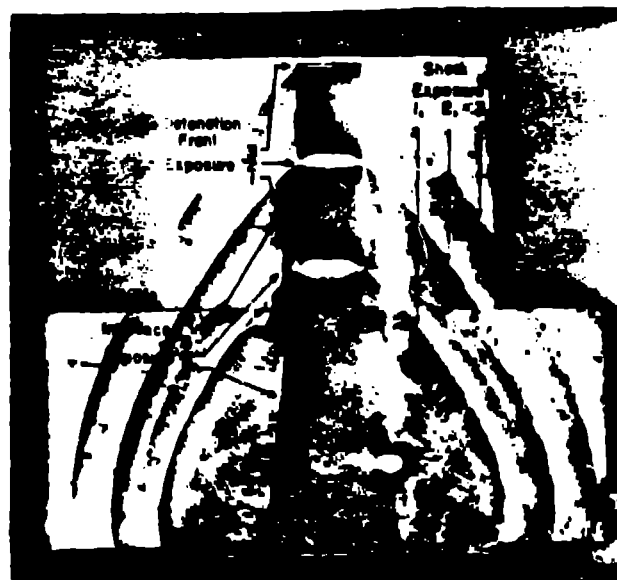


Fig. 2. Shot C-4632; 10-cm-diameter ANFO cylinder with Plexiglas confinement. Three I²C exposures.

of 3.9 km/s measured by Helm et al.⁹ for a 10-cm-diameter charge.

Based on ideal performance calculations using the theoretical explosive chemistry code BKW,¹⁴ the detonation velocity for ANFO should be 5.44 km/s with a detonation pressure of 7.3 GPa, if the reaction were complete. Comparison with the measured detonation speed shows that conditions are far from ideal. When we go to a 20-cm-diameter cylinder with clay-pipe confinement (shot C-4634), the detonation velocity increases to 4.12 km/s. Conditions are tending toward ideal, but still have a substantial way to go. Measurements made by Helm et al.⁹ show that detonation velocities in ANFO are also well below ideal conditions for charge diameters of 5.1 cm, 10.2 cm, and 29.2 cm. In fact, field data⁹ on a 550-cm charge of ANFO give a detonation velocity of only 4.7 km/s. Hence, even for extremely large charges, the detonation velocity remains considerably below the value predicted by the BKW code under the assumption of complete reaction. Persson,¹⁵ however, reports detonation velocities in ANFO very close to the theoretical value of 5.44 km/s for 26.8-cm charges confined in rock.

Therefore, we conclude that the detonation velocity data obtained on 10- and 20-cm-diameter ANFO charges are consistent with existing data, and that reactions in these geometries are nonideal. In addition, water-tank data can be used to quantify these effects.

To describe the observed explosive properties of ANFO, it is assumed that some fraction of the candidate reactants do not participate in the chemical reaction at the detonation front. A theoretical (BKW)¹⁴ detonation speed of 3.5 km/s is obtained if it is assumed that 55% of the ammonium nitrate remains inert at the detonation front. This agrees with measured velocity for the 10-cm-diameter ANFO water-tank test, and gives a C-J pressure of 24 kbar.

Based on the explosive equation of state for 55%-inert ANFO, a finite-difference calculation of shot C-4632 is performed with the two-dimensional Lagrangian code 2DL.¹⁶ A comparison of the theoretical and experimental results is shown in Fig. 3, where it is seen that both the measured shock-wave and Plexiglas/water interface positions are in poor agreement with the calculation.

Several additional BKW calculations were then performed to determine the release isentrope from the 2.4-GPa C-J point under the assumption that the AN continues to react. Based on the assumption that all of the remaining (55%) AN is reacted by the time the pressure has dropped to 10 kbar behind the detonation wave, a new release isentrope is calculated and used in a second calculation of water-tank shot C-4632. Figure 4 shows the results. Note that both the shock and interface positions are in better agreement with the experimental data. These results are not sensitive to the precise way in which the remaining AN is assumed to undergo reaction.

The conclusion is that 55% of the ammonium nitrate remains inert at the detonation front in a 10-cm-diameter ANFO cylinder, but reacts shortly

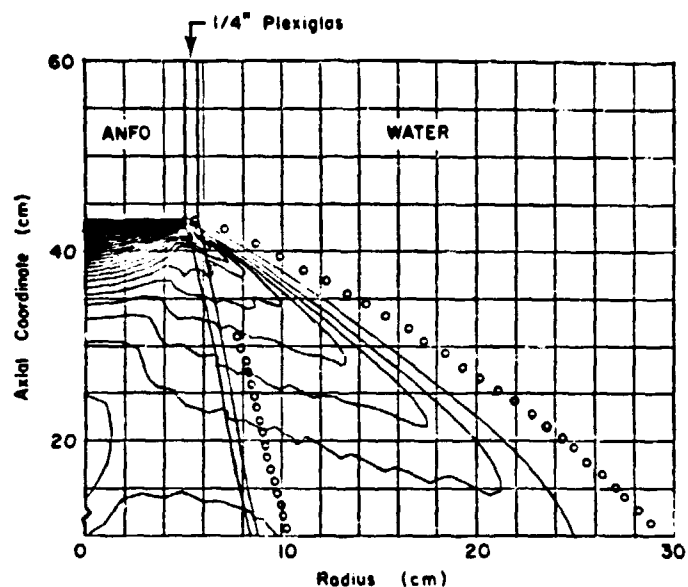


Fig. 3. Shot C-4632; comparison of measured (circles) shock and interface positions with those calculated assuming that 55% of the AN remains inert behind the detonation front. The contours are the calculated pressures at 0.1 GPa intervals.

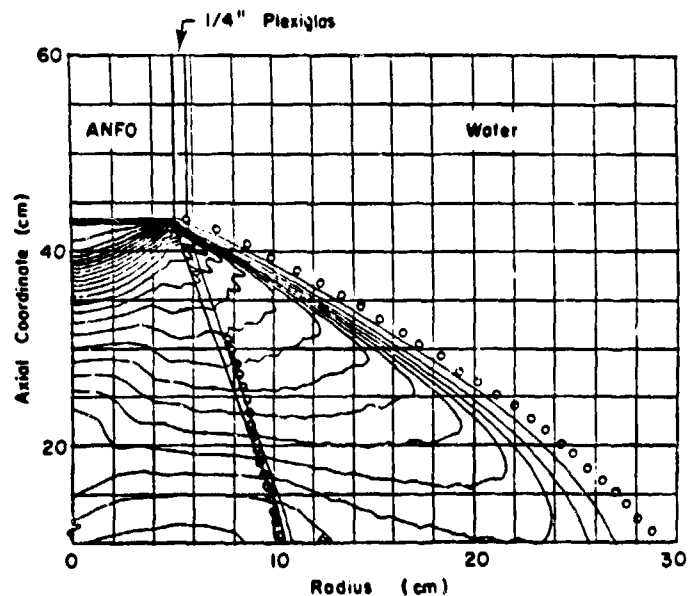


Fig. 4. Shot C-4632; comparison of measured (circles) shock and interface positions with those calculated assuming that all of the remaining (55%) AN reacts by the time the pressure drops to 10 kbar. The contours are the calculated pressures at 0.1 GPa intervals.

after the passage of the detonation wave (i.e., within a few microseconds).

Water-tank experiments on 20-cm-diameter ANFO cylinders in 2.2-cm-thick clay pipe yield detonation velocities of 4.1 km/s corresponding to 38% of the ammonium nitrate remaining inert at the detonation front. Comparison of two-dimensional finite-difference calculations with measured shock and clay-pipe/water interface positions indicate that complete reaction is again achieved within a few microseconds after the passage of the detonation wave.

Chapman-Jouguet states and release adiabats for 10-cm, 20-cm, and $> \sim 30$ -cm-diameter ANFO charges are shown in Fig. 5. These pressure-volume states give the correct detonation speed as a function of diameter, and accurately simulate other features of the water-tank experiments. The sudden change in slope for the 10-cm and 20-cm-diameter cases (dashed and dotted lines) corresponds to completion of the ammonium nitrate reaction behind the

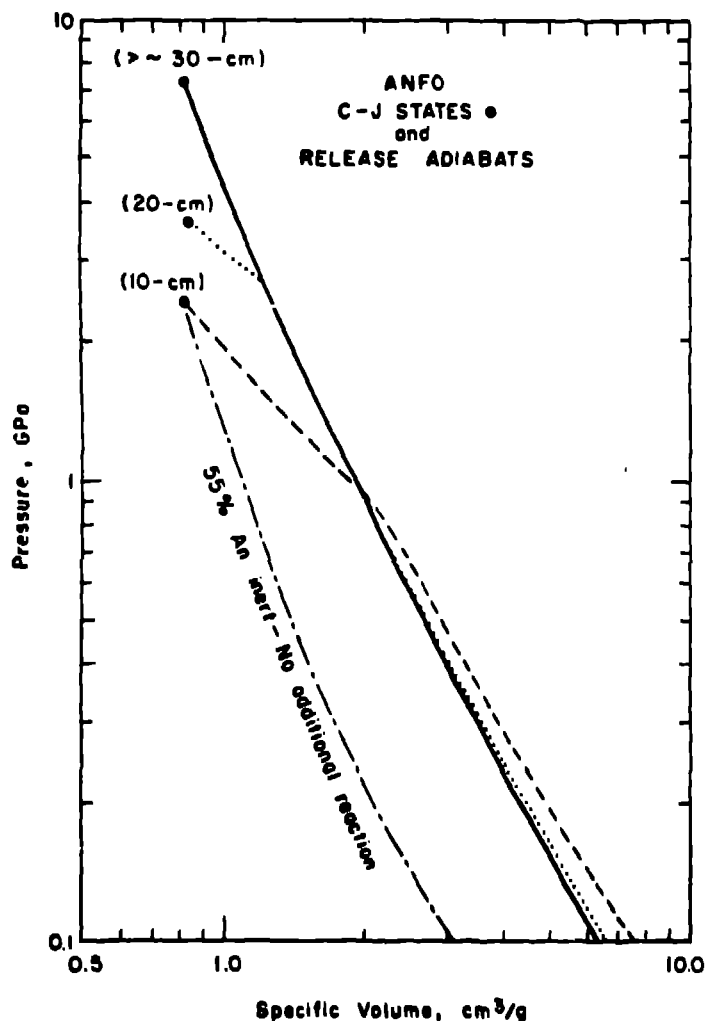


Fig. 5. Calculated C-J states and release adiabats for cylindrical ANFO charges of various diameters.

detonation front. In all cases (10-, 20-, and $> \sim 30$ -cm diameters) the total energy released is the same. Also shown in Fig. 5 is the calculated release adiabat for the 10-cm-diameter ANFO cylinder assuming that the unreacted (55%) ammonium nitrate remains inert behind the detonation front. In this case the total energy released is much less and accounts for the large difference between the calculations in Figs. 3 and 4.

In the rock breakage calculations described here, separate logarithmic fits are made to the complete thermodynamic equation of state for ANFO at 10-cm, 20-cm, and larger ($> \sim 30$ -cm) diameters, as discussed in Ref. 16. These equations of state are then used in the two-dimensional fracture calculations presented in this paper.

CONSTITUTIVE PROPERTIES OF INTACT AND FRACTURED OIL SHALE

The properties considered here are (1) elastic moduli, (2) high-pressure Hugoniot response, (3) the failure surface for intact rock, and (4) loss of strength in partially and fully fractured rock. All properties are correlated with initial density or, equivalently, kerogen content.¹⁷ Only those data pertaining to oil shale obtained from the Anvil Point Mine near Rifle, Colorado, are included in development of the material constitutive description. Consequently, the data presented here are not intended to be a complete summary of all available information on the mechanical properties of oil shale.

Experimental data have been collected from various sources for determination of mechanical properties of Anvil Point oil shale of approximately 1.4 g/cm³ (> 80 gal/ton kerogen content) to 2.5 g/cm³ (~ 10 gal/ton kerogen content). Ultrasonic data at zero confining pressure give average isotropic shear (μ) and longitudinal (C_{11}) moduli as functions of initial density according to the following relationships:

$$\mu(\text{GPa}) = \begin{cases} \rho_0 [1.45 + 0.59(\rho_0 - 1.4)]^2, & (\text{for } 1.4 < \rho_0 < 2.0 \text{ g/cm}^3) \\ \rho_0 [1.80 + 2.63(\rho_0 - 2.0)]^2, & (\text{for } 2.0 < \rho_0 < 2.5 \text{ g/cm}^3) \end{cases} \quad (1)$$

$$C_{11}(\text{GPa}) = \begin{cases} \rho_0 [2.80 + 0.5(\rho_0 - 1.4)]^2, & (\text{for } 1.4 < \rho_0 < 2.0 \text{ g/cm}^3) \\ \rho_0 [3.1 + 4.1(\rho_0 - 2.0)]^2, & (\text{for } 2.0 < \rho_0 < 2.5 \text{ g/cm}^3) \end{cases} \quad (2)$$

These equations are obtained by simple numerical averaging of two shear wave velocities, V_4 (I) and V_6 (II), and three longitudinal wave velocities, V_1 (II), V_3 (I), and V_5 (45°), obtained by Olinger.¹⁸ The dependence of ultrasonic wave speeds on propagation direction and polarization is a consequence of elastic anisotropy. Here V_1 (II), V_3 (I), and V_5 (45°) are longitudinal wave speeds parallel, perpendicular, and 45° to the bedding planes, while V_4 (I) and V_6 (II) are shear wave velocities perpendicular and parallel to the bedding planes, with the polarization of V_6 (II) also parallel to the bedding planes. In the calculations presented here

elastic anisotropy is ignored because anisotropic effects tend to become less pronounced at higher pressures (i.e., those encountered in explosive loading) and because we do not yet have a very complete picture of anisotropic effects on fracture.

High-pressure shock-wave experiments¹⁹ show that the shock velocity U_s and particle velocity u behind the shock front are related linearly according to

$$U_s = c_0 + su \quad (3)$$

where $c_0 = [(C_{11} - 4\mu/3)/\rho_0]^{1/2}$ is the low-pressure bulk sound speed from Eqs. (1) and (2), and $s \approx 1.5$ independent of initial density. Equation (3) defines the nonlinear pressure/volume behavior of oil shale at high pressure. This gives the following pressure/volume relationship for the Hugoniot curve:

$$P = \rho_0 c_0^2 [1 - V/V_0] / [1 - s[1 - V/V_0]]^2 \quad (4)$$

Thermal properties affect the shock compression of oil shale only slightly but they are included in the calculations. The values of specific heat c_v , linear coefficient of thermal expansion α , and the Grüneisen constant Γ_0 are assumed to be independent of initial density and to be given by

$$c_v = 0.3 \text{ cal/g} \quad ,$$

$$\alpha = 0.5 \times 10^{-6} \quad ,$$

$$\Gamma_0 = 1.4 \quad .$$

The remaining properties that must be defined are those related to shear failure. The yield strength of Anvil Point oil shale has been determined as a function of mean stress and initial sample density to be²⁰

$$Y = Y_0 + \Delta Y (1 - e^{-ap}) \quad (5)$$

where Y is the yield strength and p is the mean stress. For general three-dimensional loading states,

$$Y = \sqrt{(3/2)s_{ij}s_{ij}} \quad ,$$

where the s_{ij} are components of the stress deviator and a repeated index implies summation.

Equation (5) gives a good fit to the failure surface over the range of initial densities of 2.0 g/cm³ to 2.25 g/cm³ as shown in Fig. 6. The parameters Y_0 , ΔY , and a depend on initial density according to Fig. 7. Also presented in Fig. 7 is the approximate value of p^* (the pressure at which the transition from brittle to ductile inelastic deformation occurs) as determined from the results of Heard²¹ and Simonson et al.²² Heard finds p^* at the brittle-ductile transition in 2.19- and 2.28-g/cm³ oil shale to be approximately 0.1 and 0.5 GPa, respectively. Triaxial tests by Simonson et al. indicate a somewhat lower value for p^* in the 2.25-g/cm³ material. Generally, determination of unambiguous values of p^* as a function of density is difficult in terms of the present data, and the straight line shown in Fig. 7 is means as only a very gross approximation. For example, the value of $p^* = 0.1$ GPa in 2.0-g/cm³ oil should be thought of only as an upper limit. Laboratory measurements to determine the value of p^* as a function of material density more precisely would be very useful.

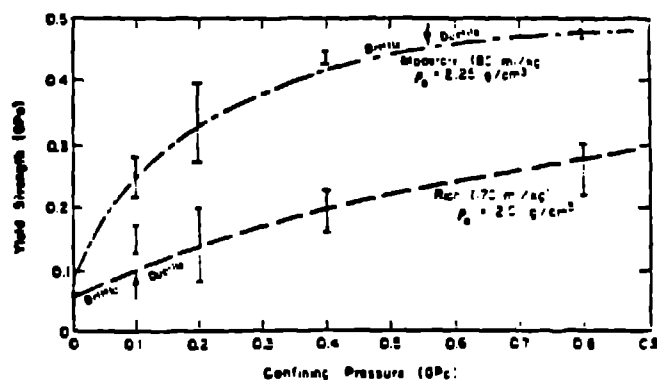


Fig. 6. Yield strength of 2.0- and 2.25-g/cm³ oil shale as a function of confining pressure. Also indicated is the approximate position of each "brittle/ductile" transition.

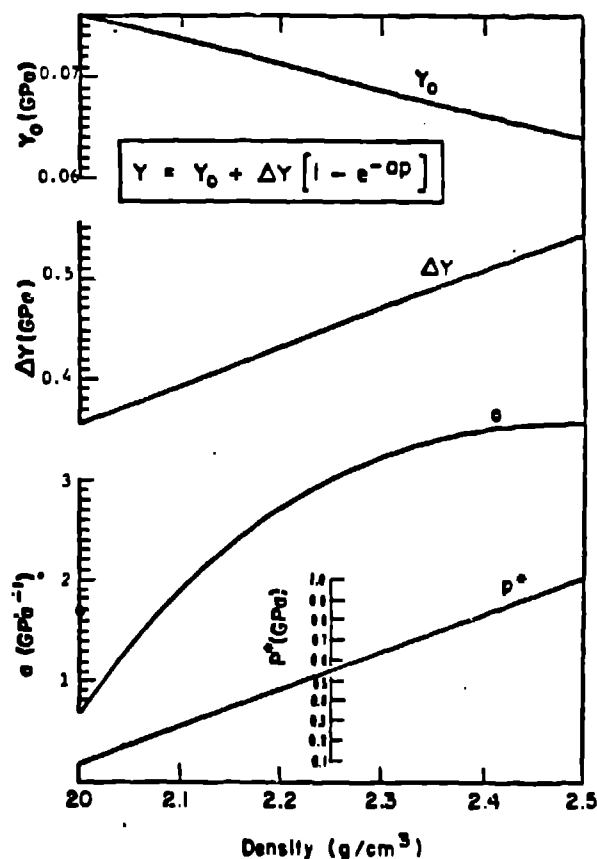


Fig. 7. Parameters in the relationship between yield stress Y and mean stress p as functions of sample density.

The equation of state, or constitutive relation, for oil shale used in the two-dimensional Lagrangian calculations of explosive loading is then

given in terms of the hydrostatic pressure rate \dot{p} and deviatoric stress rate \dot{s}_{ij} according to

$$\dot{p} = \rho_0 c_0^2 (1 - \alpha c_v)^{-3} (1 + \alpha c_v - \Gamma_0 c_v) (\dot{c}_v - \dot{c}_v^p) + \rho_0 \Gamma_0 \dot{I} \quad (14)$$

$$\dot{s}_{ij} = 2\mu(\dot{e}_{ij} - \dot{e}_{ij}^p) - t_{ij} \quad (15)$$

where c_v and e_{ij} are the total volumetric and deviatoric strain components. In Eq. (14) ρ_0 is the initial density, c_0 is the zero-pressure bulk sound speed, α is the straight-line slope relating shock velocity to particle velocity, Γ_0 is the Grüneisen parameter, I is the specific internal energy. In Eq. (15) μ is the shear modulus, and t_{ij} corrects \dot{s}_{ij} for the rotation rate of the Lagrangian coordinate system as defined previously.¹⁶

To represent rate-dependent material behavior, the term $\dot{\lambda}$ is written as

$$\dot{\lambda} = b \Delta S \quad (16)$$

where b (units of stress⁻² time⁻¹) is a constant and ΔS is a scalar quantity specifying the departure of the stress state from the static failure envelope. For $p \geq p_c$ we have chosen $\Delta S = Y' - g(p, D)$ and for $p < p_c$ the quantity ΔS is determined by the straight-line distance (in stress space) from point p', Y' to point A shown in Fig. 8.

The rate at which damage accumulates depends on the rate of inelastic deformation below the brittle/ductile point defined by the mean stress p^* . For mean stresses greater than p^* , oil shale deforms in a ductile manner without fracturing and loss of strength. It might also be expected that the damage accumulation rate decreases as D approaches 1. That is, it is harder to create additional damage in an already fractured rock than it is in an intact, or nearly intact, specimen.

A mathematical expression for D that contains these ideas is given by

$$\begin{aligned} \dot{D} &= \xi \dot{\lambda} (1 - D) (1 - p/p^*) \quad \text{for } p < p^* \\ \dot{D} &= 0 \quad \text{for } p \geq p^* \end{aligned} \quad (17)$$

Here ξ is a scalar quantity (with units of stress) to be determined by comparison of finite-difference calculations with field and laboratory experiments.

FINITE-DIFFERENCE CALCULATIONS

Numerical calculations of explosive rock breakage are performed with the two-dimensional finite-difference code 2DL.¹⁶ This code gives a solution to the coupled set of partial differential equations of mass, momentum, and energy conservation combined with the explosive equation of state and material constitutive description presented in the previous section.

In all calculations shown here the oil shale density is taken to be 2.25 g/cm³, corresponding to a kerogen content of approximately 20 gal/ton.¹⁷ The thermoelastic and failure surface parameters are then found to be, from the previous section:

$$\begin{aligned} \mu &= 13.6 \text{ GPa} \\ c_{11} &= 38.3 \text{ GPa} \end{aligned}$$

$$\begin{aligned} c_0 &= 0.30 \text{ cm/us} \\ \alpha &= 1.5 \\ \Gamma_0 &= 1.4 \\ c_v &= 0.3 \text{ cal/g} \\ Y_0 &= 0.07 \text{ GPa} \\ \Delta Y &= 0.45 \text{ GPa} \\ a &= 3 \text{ GPa}^{-1} \end{aligned}$$

The only unknown material parameters are b in Eq. (16) and ξ , the damage accumulation rate constant in Eq. (17). A value of $b = 0.1 \text{ GPa}^{-2}$ is chosen to give the largest allowable rate of relaxation to $Y = g(p, D)$ such that the numerical solution remains stable and, therefore, closely represents rate-dependent material response.

The first calculation simulates a cratering experiment conducted in the floor of the Colony Mine near Rifle, Colorado.²⁴ Here a 10-cm-diameter ANFO charge (65-cm long) was placed 129 cm below the free surface (to the top of the charge) and detonated from the bottom. The charge hole was stemmed with crushed oil shale. The calculated damage pattern at $t = 1.14$ ms (with $\xi = 50 \text{ GPa}$ and $p^* = 0.1 \text{ GPa}$) is shown in Fig. 9 in relationship to the observed crater. This value of p^* is less than given by the graph in Fig. 7 because the average kerogen content of this material was thought to be somewhat richer than 20 gal/ton. A highly rubblized zone ($D > 0.7$) of broken rock occurs next to the free surface directly above the explosive charge, with modest ($0.3 < D < 0.7$) and low ($0.1 < D < 0.3$) level damage extending to greater depth around the borehole. These observations give a qualitative representation of the fragment size distribution in the rubble pile.

It is seen that the theory predicts an unbroken region in the immediate vicinity of the borehole. Because of the very high confining pressures in this region ($> 0.1 \text{ GPa}$) the inelastic deformation was ductile. The final hole diameter is calculated to be 17.6

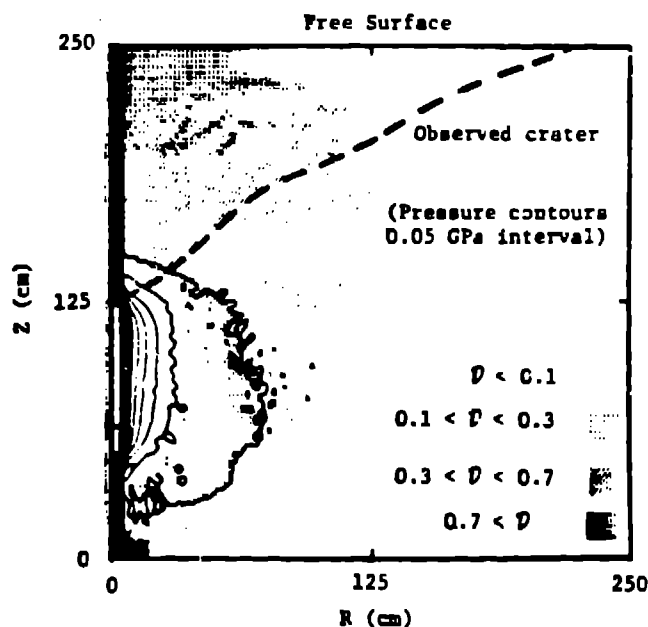


Fig. 9. Calculated damage pattern for 10-cm-diameter ANFO charge in oil shale.

cm. The measured final diameter (>20 cm) was difficult to determine because of flaking of the wall, indicating that some degree of rubblization may have occurred near the cavity.

The damage pattern of Fig. 9 shows only the very early breakage due to the first passage (and reflection from the free surface) of the explosively generated shock wave. At $t = 1.14$ ms there remains a pressure of ~ 0.4 GPa (~ 60 ksi) in the borehole and this would be expected to drive a large conical-shaped crack to the surface. Consideration of how a large scale crack propagates to the surface is the subject of current investigation.

The second set of calculations has to do with bench blasting in planar geometry. A 15-cm-thick ANFO slab (1-m long) is placed 60 cm from a free corner as shown in Fig. 10A. The performance properties of ANFO are interpolated from data on the 10-cm- and 20-cm-diameter water-tank tests. Here the parameters ξ and p^* are taken to be 10 GPa and 0.5 GPa, respectively. The key to the shaded regions is the same as for Fig. 9.

In blasting to a free volume (Fig. 10A) highly fractured regions are produced near the free surfaces, both directly below and to the right of the explosive charge. In addition, a highly fractured region is produced between the upper right corner of the explosive and the free corner, thus indicating that a clean break should be produced from the top of the explosive charge to the free corner.

A second case was studied in which rubblized oil shale (20% porous, with corresponding reduction in moduli) was placed in the region 60 cm to the right of the planar charge; Fig. 10B. The effect of dense rubblized rock was to inhibit intensive breakage to the right of the charge, but not to change substantially the damage pattern extending from the top of the charge to the corner. These interpretations are dependent on the correct assignment of parameters ξ and p^* , and therefore should not be considered firm on the basis of existing data. Also, for actual field applications, a row of cylindrical explosive charges is generally used instead of the ideal planar charge. Proper simulation of distributed cylindrical charges is also necessary before such planar calculations can be considered representative.

SUMMARY

Successful calculation of explosive rock breakage requires knowledge of commercial explosive performance and material constitutive properties of intact and fractured rock. The nonideal performance properties of ANFO are presented here as a function of charge diameter and are used in calculations of field experiments. A summary of rock properties is presented for Anvil Point oil shale as functions of density or, alternatively, kerogen content. These data are then combined with a continuous model of rock fracture, and several two-dimensional finite-difference calculations are performed for crater and bench blasting geometries.

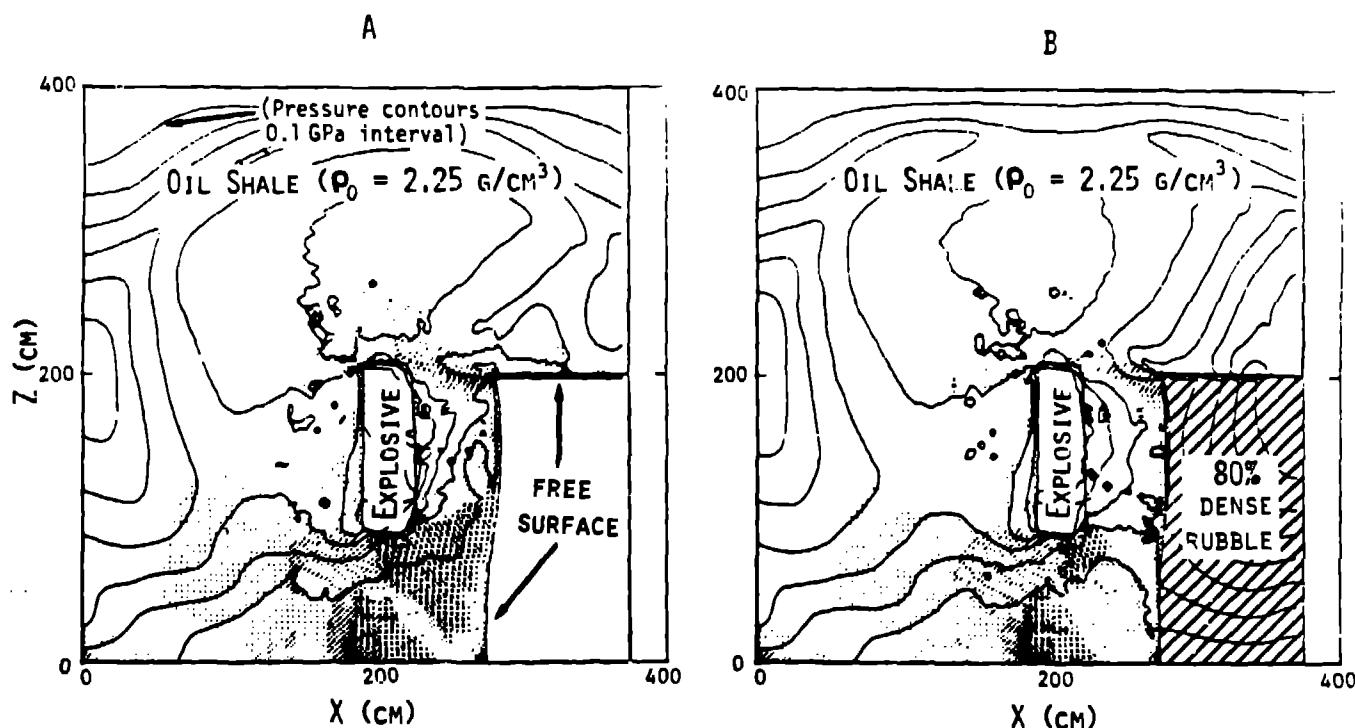


Fig. 10. Calculated damage patterns for 15-cm-thick planar ANFO charge 60 cm from (A) free corner, (B) 80% dense rubble.

These calculations show the expected spatial location of the fracture damage produced on the single (or direct and reflected) passage of the stress wave which comes from the explosive source. The calculation also gives the equilibrium pressure in the borehole on the order of a millisecond after explosive initiation. What is presently lacking in such a calculation is a description of how this residual pressure (~ 0.4 - 0.5 GPa, or 60-75 ksi) drives large-scale cracks to a nearby free surface.

If we think of explosive rock fragmentation as the two separate and distinct processes of (i) rubbleization and fragmentation on the first passage (direct and reflected) of the initial shock wave, and (ii) large-scale crack propagation to a free surface, then additional calculations can perhaps be performed to follow the propagation of individual cracks perpendicular to the late-time (>1 ms) minimum principal (tensile) stress. The initial conditions for such calculations would be obtained from damage calculations, such as shown in Figs. 9 and 10, after approximately 1 μ s. These effects are presently being investigated.

REFERENCES

1. C. H. Noren and D. C. Porter, "A Comparison of Theoretical Explosive Energy and Energy Measured Under Water with Measured Rock Fragmentation," in Advances in Rock Mechanics, Vol. III, Part B (Nat. Acad. Sci., 1974).
2. W. I. Duvall and T. C. Atchison, "Rock Breakage by Explosives," US Bureau of Mines report R.I. 5336 (1957).
3. U. Langefors and V. Kihlstrom, The Modern Technique of Rock Blasting (John Wiley and Sons, Inc., New York, 1963).
4. C. H. Johansson and P. A. Persson, Detonics of High Explosives (Academic Press, New York, 1970).
5. P. A. Persson, N. Lundberg, and C. H. Johansson, "The Basic Mechanisms in Rock Blasting," in Proc. 2nd Cong. Int. Soc. Rock Mech. (Beograd, 1970), p. 1.
6. B. G. Craig, J. N. Johnson, C. L. Mader, and G. F. Lederman, "Characterization of Two Commercial Explosives," Los Alamos Scientific Laboratory report LA-7140 (May 1978).
7. O. G. Winslow, W. C. Davis, and W. C. Chiles, "Multiple-Exposure Image-Intensifier Camera," Proc. Symp. Detonation, 6th, August 1976, pp. 197-200.
8. E. L. Lee, H. C. Hornig, and J. W. Kury, "Adiabatic Expansion of High Explosive Detonation Products," Lawrence Livermore Laboratory report UCRL-50422 (May 1968).
9. F. Helm, M. Finger, B. Hayes, E. Lee, H. Cheung, and T. Walton, "High Explosive Characterization for the Dice Throw Event," Lawrence Livermore Laboratory report UCRL-52042 (June 1976).
10. L. Pann, F. Helm, M. Finger, and E. Lee, "Determination of Equation-of-State Parameters for Four Types of Explosive," Lawrence Livermore Laboratory report UCRL-51892 (August 1975).
11. J. Hershkowitz and J. Rigdon, "Evaluation by a Modified Cylinder Test of Metal Acceleration by Nonideal Explosives Containing Ammonium Nitrate," Picatinny Arsenal report PA-TR-4611 (April 1974).
12. N. L. Coleburn, H. D. Jones, and H. M. Sternberg, "Initiation, Detonation Propagation, Computational Studies for Submunitions Containing Amatex-20," Naval Surface Weapons report TR 75-94, White Oak Laboratory (February 1976).
13. C. L. Mader, "An Equation of State for Nonideal Explosives," Los Alamos Scientific Laboratory report LA-5864 (April 1975).
14. C. L. Mader, "FORTRAN BKW: A code for Computing the Properties of Explosives," Los Alamos Scientific Laboratory report LA-3704 (July 1967).
15. P. A. Persson, "Swedish Methods for Mechanized Blasthole Charging," AIIME Preprint No. 75-AO-74 (1975).
16. C. L. Mader, Numerical Modeling of Detonations (University of California Press, Berkeley, CA, 1978).
17. J. Ward Smith, "Specific Gravity - Oil Yield Relationships of Two Colorado Oil Shale Cores," Ind. and Engineering Chem., Vol. 48, 441 (1956).
18. B. Olinger, "Elastic Constants of Oil Shale," Los Alamos Scientific Laboratory report LA-6817-PR, pp. 24-26 (Sept. 1977).
19. W. J. Carter, "Hugoniot of Green River Oil Shale," Los Alamos Scientific Laboratory report LA-6817-PR, pp. 2-6 (Sept. 1977).
20. J. N. Johnson and E. R. Simonson, "Analytical Failure Surfaces for Oil Shale of Varying Kerogen Content," Sixth AIRAPT International High-Pressure Conference, Boulder, CO, July 1977.
21. H. C. Heard, "The Influence of Environment on the Inelastic Behavior of Rocks, Proc. Symp. Engineering with Nuclear Explosives, Jan. 14-16, 1970, Las Vegas, Nevada (Am. Nuclear Society report CONF-700101, Vol. 1, p. 127).
22. E. R. Simonson, J. N. Johnson, and L. Buchholdt, "Anisotropic Mechanical Properties of a Moderate and Rich Kerogen Content Oil Shale," Terra Tek report TR 76-72 (December 1976).
23. K. W. Schuler, personal communication.
24. S. C. Schmidt, C. C. Edwards, J. N. Johnson, R. Oliver, and P. Wapner, "Empirical Characterization of Oil Shale Fragmentation Experiments," presented at the Fifth Annual Conference on Explosives and Blasting Technology, St. Louis, February 1979.